JOURNAL OF GEOPHYSICAL RESEARCH, VOL. 115, B06314, doi:10.1029/2009JB007134, 2010

Lamé parameters of common rocks in the Earth's crust and upper mantle

Shaocheng Ji,[1] Shengsi Sun,[1] Qian Wang,[2] and Denis Marcotte[1]

Received 13 November 2009; revised 15 January 2010; accepted 28 January 2010; published 24 June 2010.

[1] Lamé parameter (λ) and shear modulus (μ) are the most important, intrinsic, elastic properties of rocks. The Lamé parameter λ, which relates stresses and strains in perpendicular directions, is closely related to the incompressibility and contains a high proportion of information about the resistance to a change in volume caused by a change in pressure. Recent studies have emphasized the roles played by λ in the discrimination of gas sands from carbonates and shale in sedimentary basins and in the seismic reflection of crustal fault zones. Here we analyze the equivalent isotropic elastic data of 475 natural rocks in order to characterize λ values for common types of crystalline rocks in the Earth's crust and upper mantle and their variations with pressure (P), temperature (T), and mineralogical composition. When no partial melting, metamorphic reaction, dehydration, or phase transformation occurs, λ of a crystalline rock as a function of P and T can be described by $\lambda = a + (\mathrm{d}\lambda/\mathrm{d}P)P - c\exp(-kP) - (\mathrm{d}\lambda/\mathrm{d}T)T$, where a is the projected λ value at zero pressure if microcracks were fully closed; $\mathrm{d}\lambda/\mathrm{d}P$ is the pressure derivative in the linear elastic regime; c is the initial λ drop caused by the presence of microcracks at zero pressure; k is a decay constant of the λ drop in the nonlinear poroelastic regime; and $\mathrm{d}\lambda/\mathrm{d}T$ is the temperature derivative. The parameter λ increases nonlinearly and linearly with increasing pressure at low (<~300 MPa) and high (>~300 MPa) pressures, respectively. In the regime of high pressures, λ decreases quasi-linearly with increasing temperature with $\mathrm{d}\lambda/\mathrm{d}T$ values in the range of $1–10 \times 10^{-3}$ GPa/°C. Approaching the α-β quartz transition temperature, quartzite displays negative λ values. In the λ-ρ (density) and μ-λ plots, the main categories of lithology can be clearly distinguished. The ultramafic rocks display systematic decreases in both μ and λ with increasing the degree of serpentinization. Eclogites, mafic rocks (gabbro, diabase, mafic granulite, and mafic gneiss), and felsic rocks (granite, diorite, felsic gneiss, intermediate gneiss, and metasediments) are characterized by high, moderate, and low μ and λ values, respectively. For pyroxene and olivine, both λ and ρ increase, but μ decreases with increasing the Fe/Mg ratios. In the plagioclase series, both λ and μ increases with increasing the anorthite content. Increases in the contents of garnets, sillimanite, rutile, zircon, ilmenite, and spinel result systematically in an increase in rock's λ and μ values. The present results provide improved constraints on the discrimination of composition for crustal and upper mantle rocks in terms of λ and μ.

Citation: Ji, S., S. Sun, Q. Wang, and D. Marcotte (2010), Lamé parameters of common rocks in the Earth's crust and upper mantle, *J. Geophys. Res.*, *115*, B06314, doi:10.1029/2009JB007134.

1. Introduction

[2] The elastic properties of an isotropic material or rock can be described by two independent moduli termed lambda (λ) and mu (μ), introduced and named after the 18th century French mathematician and engineer G. Lamé (1795–1870). In 1828, Lamé formulated the modern version of Hooke's law relating stress (σ_{ij}) to strain (ε_{ij}) in its general tensor form, thereby creating the basis for the materials sciences and rock mechanics:

$$\sigma_{ij} = \delta_{ij}\lambda\Delta + 2\mu\varepsilon_{ij} \quad (1)$$

where the volume strain $\Delta = \varepsilon_{11} + \varepsilon_{22} + \varepsilon_{33}$, δ_{ij} is the Kronecker delta, $\delta_{ij} = 1$ when $i = j$, and $\delta_{ij} = 0$ when $i \neq j$; λ and μ are the first and second Lamé constants, respectively. The second Lamé constant μ is identical to the shear modulus or rigidity, which is defined as the resistance to a simple shear strain that produces a shape change without

[1]Département des Génies Civil, Géologique et des Mines, École Polytechnique de Montréal, Montréal, Québec, Canada.
[2]Key Laboratory of Marginal Sea Geology, Guangzhou Institute of Geochemistry, Chinese Academy of Sciences, Guangzhou, China.

0148-0227/10/2009JB007134

changing total volume. Hereafter we will use Lamé parameter (λ) in place of the first Lamé constant as it varies with pressure and temperature.

[3] For an isotropic medium, equation (1) can be written in matrix-vector form that is composed of 6 rows and 6 columns:

$$\begin{bmatrix}\sigma_{11}\\ \sigma_{22}\\ \sigma_{33}\\ \sigma_{12}\\ \sigma_{13}\\ \sigma_{23}\end{bmatrix} = \begin{bmatrix}\lambda+2\mu & \lambda & \lambda & 0 & 0 & 0\\ \lambda & \lambda+2\mu & \lambda & 0 & 0 & 0\\ \lambda & \lambda & \lambda+2\mu & 0 & 0 & 0\\ 0 & 0 & 0 & 2\mu & 0 & 0\\ 0 & 0 & 0 & 0 & 2\mu & 0\\ 0 & 0 & 0 & 0 & 0 & 2\mu\end{bmatrix}\begin{bmatrix}\varepsilon_{11}\\ \varepsilon_{22}\\ \varepsilon_{33}\\ \varepsilon_{12}\\ \varepsilon_{13}\\ \varepsilon_{23}\end{bmatrix} \quad (2)$$

The parameter λ relates stresses and strains in perpendicular directions [*Jaeger*, 1969]. The physical meaning of λ can be clearly illustrated in a special case of uniaxial strain where $\varepsilon_1 \neq 0$, and $\varepsilon_2 = \varepsilon_3 = 0$ (i.e., no displacement occurs perpendicular to the x axis): $\lambda = \sigma_2/\varepsilon_1 = \sigma_3/\varepsilon_1$. Interestingly and most notably, only λ and μ appear in Hooke's law, but not Young's modulus (E), the bulk modulus (K), or Poisson's ratio (υ). This indicates that λ and μ are the most intrinsic elastic coefficients to express stress in terms of strain.

[4] *Goodway* [2001] believes that λ is closely related to material's incompressibility ($\lambda = K - 2\mu/3$) and contains a higher proportion of information about the resistance to a change in volume caused by a change in pressure. The parameter μ corresponds to material's resistance to simple shear. The parameter λ is negative if $K < 2\mu/3$ as $K > 0$ and $\mu > 0$.

[5] The most common geophysical parameters measurable are compressional (P) and shear (S) wave velocities (V_p and V_s) and densities (ρ) of elastic media; λ and μ for isotropic elasticity can be easily determined from the measured seismic data:

$$\mu = \rho V_s^2 \quad (3)$$

$$\lambda = \rho(V_p^2 - 2V_s^2) \quad (4)$$

$$\lambda/\mu = \left(V_p/V_s\right)^2 - 2 \quad (5)$$

$$\lambda\rho = Z_p^2 - 2Z_s^2 \quad (6)$$

$$\mu\rho = Z_s^2 \quad (7)$$

where Z is the acoustic impedance; P wave impedance $Z_p = \rho V_p$, and S wave impedance $Z_s = \rho V_s$; $\lambda = 0$ if $V_p/V_s = \sqrt{2}$, and $\lambda < 0$ if $V_p/V_s < \sqrt{2}$; $\lambda/\mu \geq 1$ if $V_p/V_s \geq \sqrt{3}$ (e.g., serpentine, calcite, feldspar, hornblende, fayalite, dolomite), and $0 \leq \lambda/\mu < 1$ if $\sqrt{2} \leq V_p/V_s < \sqrt{3}$ (e.g., quartz, staurolite, bronzite, diallage, and enstatite). The information about the impedance or $\lambda\rho$ and $\mu\rho$ data can be extracted from the inversion of P and S wave reflectivities [*Estabrook and Kind*, 1996; *Goodway et al.*, 1997; *Goodway*, 2001; *Gray*, 2003]. *Chávez-Pérez and Louie* [1997, 1998] suggested that variations in λ control seismic reflections of crustal fault zones. Obviously, both λ and μ offer the most fundamental and orthogonal parameterization of elastic seismic waves to extract information about the composition and structure of rocks in the Earth's interior. In the literature, however, only E, K, μ, and υ are usually reported although λ is an intrinsic and invariant property of elastic media under given conditions. So far, little systematic research work has been carried out on the characterization of λ values for crystalline rocks [*Christensen*, 1966; *Kern*, 1979]. In this paper, we will investigate the pressure and temperature dependences of λ values for common categories of crystalline rocks from the Earth's crust and upper mantle, and explore the potential implications of λ as a discriminant of composition for common rock types in the Earth's crust and upper mantle. Our emphasis is placed on the properties of crystalline igneous and metamorphic rocks. For the λ values of common sedimentary rocks (i.e., sandstone, shale, limestone and dolomite) and their applications in the exploration of oil or gas reservoirs, the reader is referred to the papers of *Goodway et al.* [1997], *Goodway* [2001], *Gray and Andersen* [2000], *Dufour et al.* [2002], *Gray* [2003], and *Li et al.* [2003].

2. Data for Analysis

[6] An isotropic rock can be characterized by only two independent elastic constants: λ and μ. However, natural rocks may be elastically anisotropic due to the presence of compositional layering, lattice preferred orientation, shape preferred orientation (i.e., foliation and lineation) of rock-forming minerals and alignment of microcracks. The average elastic property of such an anisotropic rock, which is equivalent to the property of its isotropic counterpart, can be computed from the mean V_p and mean V_s values according to equations (3) and (4):

$$\overline{V}_p = \left[V_p(X) + V_p(Y) + V_p(Z)\right]/3 \quad (8)$$

$$\overline{V}_s = [V_s(XY) + V_s(XZ) + V_s(YX) + V_s(YZ) + V_s(ZX) + V_s(ZY)]/6 \quad (9)$$

In equation (8), $V_p(X)$, $V_p(Y)$ and $V_p(Z)$ are the P wave velocities along the propagation directions X, Y, and Z, respectively, which lie parallel to the stretching lineation, parallel to foliation and perpendicular to lineation, and perpendicular to foliation, respectively. In equation (9), $V_s(XY)$, $V_s(XZ)$, $V_s(YX)$, $V_s(YZ)$, $V_s(ZX)$, and $V_s(ZY)$ are the S wave velocities with the first letter in the brackets to refer to the propagation direction and the second letter to the polarization direction. Previous theoretical analyses and experimental studies [*Christensen and Ramananantoandro*, 1971; *Ji et al.*, 2003; *Wang and Ji*, 2009] suggest that the mean V_p and V_s values calculated from equations (8) and (9) give values very close to true isotropic elastic properties even in highly anisotropic rocks.

[7] The high-quality data used for the analysis were taken from a database of 475 samples on which P wave velocities

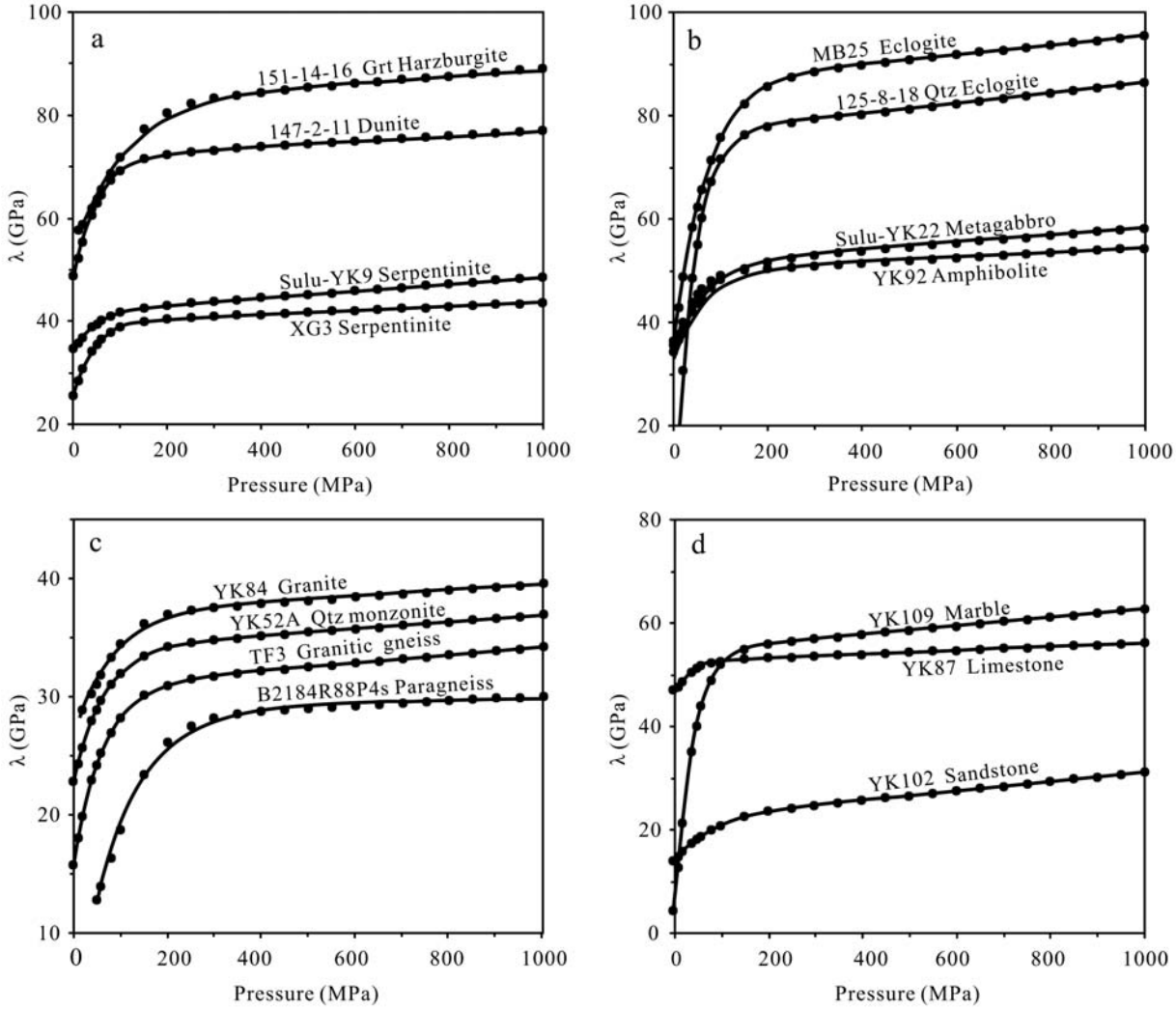

Figure 1. Lamé parameter (λ) as a function of pressure for selected lithologies from the Sulu ultrahigh-pressure metamorphic terrain (samples 151-14-16, 147-2-11, Sulu-YK9, XG3, MB25, 125-8-18, Sulu-YK22, TF3, and B2184R88P4s) and the Yunkai Mountains (samples YK52A, YK84, YK87, YK92, YK102, and YK109), China. Dots indicate experimental data; line indicates the best fitting according to equation (10) using a least squares method. Grt, garnet; Qtz, quartz.

have been well measured for the *X*, *Y*, and *Z* directions and S wave velocities for six pairs of propagation-vibration directions at high hydrostatic pressures ($\geq$ 500 MPa) using the same laboratory equipment and the same methods (i.e., the pulse transmission technique [*Birch*, 1960, *Christensen*, 1974; *Kern*, 1982]). The uncertainty of measurements is estimated to be < 0.5% for V_p, < 1% for V_s, and ±0.005 g/cm^3 for density. For each sample, λ and μ as a function of pressure or temperature were calculated. In this database, 87 samples were measured by our group: 57 from the Dabie-Sulu ultrahigh pressure metamorphic terrane and 20 from the Yunkai Mountains of China [*Wang et al.*, 2005a, 2005b; *Ji et al.*, 2007; *Wang and Ji*, 2009], and 10 from the Tantato high grade metamorphic domain in northern Saskatchewan, Canada [*Ji and Salisbury*, 1993; *Ji et al.*, 1993]. The literature data were taken from *Ji et al.* [2002, and references therein]. Only the velocities measured during depressurization were selected for the analysis because the values correspond to the stable microstructural state [*Burke and Fountain*, 1990; *Ji et al.*, 1993; *Wang et al.*, 2005a, 2005b; *Ji et al.*, 2007].

3. Results

3.1. Pressure Dependence

[8] In using λ to place constraints on lithology in the crust and upper mantle, it is necessary to understand how λ varies with pressure and temperature. Figure 1 shows typical λ-P data for common lithologies such as ultramafic rocks (peridotite, serpentinite, and partially serpentinized peridotites, Figure 1a), mafic rocks (eclogite, mafic gneiss, mafic granulite, and amphibolite, Figure 1b), felsic rocks (granite, diorite, felsic gneiss and metasediments, Figure 1c), marble and sedimentary rocks (limestone and sandstone, Figure 1d) up to 1.0 GPa, a pressure equivalent to depths of approximately 35 km. Those rocks display systematically an initial nonlinear increase in λ at low pressures followed by a more

gradual linear increase at high pressure. This phenomenon indicates that λ is strongly affected by the presence of microcracks within the rock. The rapid, nonlinear rise in λ below a critical pressure can be attributed to the progressive closure of microcracks with varying aspect ratio spectra with increasing pressure. The linear increase in λ above the critical pressure where all microcracks have been fully closed in the rock marks an elastic volume contraction of crack-free material under hydrostatic compression.

[9] The parameter λ as a function of confining pressure can be described by

$$\lambda = a + (d\lambda/dP)P - c\ \exp(-kP) \tag{10}$$

where a is the projected λ value of a nonporous or crack-free compacted rock at zero pressure, which is determined from extrapolation of the linear λ-P relationship obtained at high pressures to zero pressure; $d\lambda/dP$ is the pressure derivative in the linear elastic regime; c, which is the ambient λ drop caused by the presence of pores/microcracks at zero pressure, determines the maximum magnitude of the λ increases due to the closure of pores and microcracks; k, which is a decay constant of the λ drop, controls the shape of the nonlinear segment of the λ-P curve. The k value is a parameter to characterize the facility of the successive closure of cracks of varying aspect ratio spectra with increasing pressure. Flatter cracks yield a larger k value than more spherical pores. The zero-pressure λ value of the rock containing microcracks is the same as (a-c). In equation (10), a and $d\lambda/dP$ are two parameters which describe the λ value of the microcrack- or pore-free solid matrix, while c and k are two parameters related to the porosity and geometrical shape of pores (e.g., aspect ratio, spatial arrangement, orientation and size distribution), and in turn on the formation and deformation processes of the rocks. The same type of mathematical expression as equation (10) has been used by previous workers for describing the pressure dependence of seismic velocities [*Stierman et al.*, 1979; *Zimmerman et al.*, 1986; *Eberhart-Phillips et al.*, 1989; *Shapiro*, 2003; *Wang et al.*, 2005a, 2005b; *Ji et al.*, 2009; *Wang and Ji*, 2009]. The equation can be derived based on an assumption that the difference between the property (e.g., seismic velocities or elastic moduli) of a nonporous material and its porous counterpart at a given confining pressure has a maximum value (c) at $P = 0$ and then decays progressively with increasing P at a rate proportional to the value of the property at the applied confining pressure [*Ji et al.*, 2007]. The last term of equation (10) possesses the same form of the expression that is commonly used to describe natural phenomena such as radioactivity decay, cooling, and vibration attenuation.

[10] We used equation (10) to curve fit λ-P data for 57 samples collected from the Dabie-Sulu ultrahigh pressure (UHP) metamorphic belt using a least squares method and gave excellent results with well-constrained a, $d\lambda/dP$, c and k parameters. Table 1 lists such parameters, together with the data of density and modal composition, for only 27 representative UHP samples: 17 from the boreholes of the Chinese Continental Scientific Drilling project [*Ji and Xu*, 2009] and 10 samples from the surface quarries. The information about the locality and recovery depth for these samples were presented in *Wang et al.* [2005a, 2005b], *Ji et al.* [2007], and *Wang and Ji* [2009]. Based on the values reported in Table 1, extrapolation and interpolation can be easily performed using equation (10).

3.2. Effect of Temperature

[11] Laboratory data on the effect of temperature on seismic wave velocities and density of rocks are rather limited and were mainly from H. Kern's laboratory. Figure 2 presents the λ values as a function of temperature at a confining pressure of 600 MPa for some common rocks from the upper mantle and the continental crust. The λ values were calculated using the mean V_p and V_s data reported by *Barruol* [1993], *Kern et al.* [1999], *Kern et al.* [2002], and *Kern and Tubia* [1993]. When no partial melting [*Spetzler and Anderson*, 1968], metamorphic reaction, dehydration or phase transformation [*Kern*, 1982] occurs, most solid rocks such as garnet peridotite, harzburgite, and pyroxenite (Figure 2a), eclogites (Figure 2b), amphibolites (Figure 2c), and gabbro, granite, and granitic gneiss (Figure 2d) display that λ decreases linearly with increasing temperature due to thermal effects (e.g., thermal dilatation of mineral lattices, microcracking and grain boundary widening induced by differential thermal expansion). The gradual decrease in λ occurs over the range from room temperature to 600°C, which can be easily understood from equation (4) because dV_p/dT is significantly larger than dV_s/dT for most rocks [*Kern and Tubia*, 1993; *Kern et al.*, 1996; *Kern et al.*, 1999; *Ji et al.*, 2002; *Kern et al.*, 2002]. For basalt, however, the temperature dependence is negligible in the range from room temperature up to 600°C (Figure 2d and Table 2) probably because the elastic velocities in basaltic glass at a hydrostatic pressure of 600 MPa increase with temperature due to reduction of porosity [*Kern*, 1982].

[12] Thus, the λ-T relationship for crystalline rocks can be described by a linear equation:

$$\lambda = \lambda_0 - (d\lambda/dT)T \tag{11}$$

where λ_0 is the projected λ value when T = 0°C, and $d\lambda/dT$ is the temperature derivative. The values λ_0 and $d\lambda/dT$ as well as the modal composition for each sample illustrated in Figure 2 are given in Table 2. For these samples, $d\lambda/dT$ varies generally from 3×10^{-3} to 10×10^{-3} GPa/°C.

[13] Thus, the laboratory experimental results can be extrapolated into the Earth's interior using the following equation if there is no partial melting, metamorphic reaction, dehydration or phase `transformation:

$$\lambda(P,T) = a + (d\lambda/dP)P - c\exp(-kP) - (d\lambda/dT)T \tag{12}$$

The results computed from equation (12) have the potential of providing valuable constraints on the interpretation of the lithological and mineralogical composition of the Earth's crust and upper mantle.

3.3. Effect of α-β Quartz Transition

[14] A quartzite is taken as an example to illustrate the effect of phase transition on λ. Figure 3a presents the mean V_p and V_s data as a function of temperature at a confining pressure of 600 MPa for an ultramylonitic quartzite (89SB114a) consisting of 100% quartz. This sample was collected from a ductile shear zone in the Saint Barthelemy

Table 1. Densities, Modal Compositions, and Four Coefficients to Describe the Lamé Parameter λ for 27 Typical Samples From Dabie-Sulu UHP Metamorphic Belt, China

Sample	Lithology[a]	Density (g/cm^3)	Modal Composition[a] (vol %)	Coefficients of Lamé Parameter[b]			
				a (GPa)	$d\lambda/dP$	c (GPa)	k (GPa^{-1})
203-5-15	Amphibolite	3.07	Pl 35.0, Amp 41.0, Bt 15.0, Qtz 8.0, Chl 1.0	32.22	3.32	22.69	13.07
B1651R37P41c	Amphibolite	3.00	Amp 48.0, Chl 13.0, Grt 3.0, Cpx 15, Pl 12.0, Qtz 5.0, Ep 2.0, Opq 2.0	49.44	3.81	6.98	14.51
178-6-6	Bt dioritic gneiss	2.74	Pl 49.0, Qtz 37.0, Bt 12.0, Opq 2.0	34.27	4.32	18.93	11.19
B2184R88P4s	Bt-Hbl-Pl-Kfs paragneiss	2.66	Pl. 40.0, Kfs 15.0, Qtz 40.0, Bt 4.0, Opq 1.0	29.03	0.80	26.57	9.93
B1578R14P18t	Bt-Mus-Pl-Kfs orthogneiss	2.65	Pl 40.0, Kfs 25.0, Qtz 25.0, Mus 4.0, Bt 3.0, Grt 1.0, Opq 2.0	29.71	3.04	35.45	20.63
MB22	Coarse-grained eclogite	3.50	Grt 63.0, Cpx 35.0, Rt 1.5, Qtz 0.5	74.79	5.25	12.91	10.65
MB25	Coarse-grained eclogite	3.59	Grt 65.0, Cpx 33.0, Rt 1.5, Qtz 0.5	86.67	8.84	50.94	14.54
MB26	Coarse-grained eclogite	3.56	Grt 70.0, Cpx 29.0, Rt 0.8, Qtz 0.2	90.46	7.75	20.79	8.36
147-2-11	Dunite	3.16	Ol 88.0, Srp11.0, Opq 1.0	71.89	5.11	24.07	19.41
B2078R63P9r	Felsic orthogneiss	2.63	Pl 31.0, Kfs 35.0, Qtz 25.0, Bt 4.0, Amp 4.0, Opq 1.0	31.38	1.41	65.20	36.74
B1694R49P7s	Felsic orthogneiss	2.63	Pl 30.0, Kfs 42.0, Qtz 21.0, Cpx 4.0, Amp1.5, Opq 1.0, Rt 0.5	39.31	0.00	24.42	3.81
SB1	Fine-grained eclogite	3.37	Grt 33.0, Cpx 60.0, Amp 2.0, Rt 2.0, Qtz 1.0, Symp 2.0	81.05	1.05	20.08	6.15
TF3	Granitic gneiss	2.66	Qtz 20.0, Pl 30.0, Kfs 42.0, Opx 4.0, Opq 1.5, Rt 0.5	30.87	3.27	15.20	16.12
26-10-17	Granitic Gneiss	2.64	Pl 32.0, Kfs 31.0, Qtz 33.0, Bt 3.0, Opq 1.0	31.82	5.28	12.87	21.33
160-12-11	Grt-Harzburgite	3.17	Ol 67.0, Opx 10.0, Cpx 13.0, Grt 4.0, Srp 4.0, Phl 2.0	67.09	5.83	74.65	28.92
151-14-16	Grt-Harzburgite	3.21	Ol 68.0, Opx 14.0, Cpx 8.0, Grt 5.0, Srp 4.0, Phl 1.0	83.41	5.31	29.64	8.88
B2242R100P16a	Hbl-Bt-Pl-Kfs paragneiss	2.66	Pl 38, Kfs 18.0, Qtz 35.0, Amp 7.5, Opq 1.5	39.52	2.81	12.36	28.81
B1628R33P24	Hbl-Mag felsic orthogneiss	2.65	Pl 38.0, Kfs 15.0, Qtz 35, Amp 7.0, Grt 1.5, Opq 2.0	36.89	2.99	12.11	12.10
150-3-20	Lherzolite	3.12	Ol 70.0, Opx 8.0, Cpx 11.0, Srp 10.0, Opq 1.0	64.92	1.28	41.98	10.17
YM1	Dolomitic marble	2.86	Dol 87.0, Cal 7.0, Qtz 4.0, Grt 1.0, Cpx 1.0	41.15	1.62	21.35	24.74
Sulu-YK3B	Metagabbro	3.00	Pl 72.0, Cpx 4.0, Grt 8.0, Qtz 4.0, Mus 9.0, Chl 3.0	50.13	3.61	16.21	21.99
Sulu-YK22	Metagabbro	2.96	Pl 45.0, Cpx 14.0, Grt 9.0, Qtz 10.0, Mus 5.0, Chl 11.0, Zo 5.0, Opq. 1.0	51.07	7.18	16.96	15.40
166-42-43	Phl dunite	3.25	Ol 86.0, Opx 2.0, Phl 4.0, Srp 5.0, Opq 3.0	63.20	4.72	24.35	16.00
315-1-11	Phn eclogite	3.43	Grt 36.0, Cpx 40.0, Amp 5.0, Phn 17.0, Qtz 1.0, Rt 1.0	80.26	0.00	45.19	12.70
125-8-18	Qtz eclogite	3.38	Grt 40.0, Cpx 35.0, Amp 4.0, Symp 12.0, Qtz 7.0, Phn 1.5, Rt 0.5	76.63	9.66	75.09	24.63
XG3	Serpentinite	2.66	Srp 80.0, Ol 15.0, Opq 5.0	40.03	3.66	14.48	23.07
Sulu-YK9	Serpentinite	2.60	Srp 85.0, Tlc 10.0, Opq 5.0	41.99	6.73	7.67	21.43

[a]Abbreviations are Amp, amphibole; Bt, biotite; Cal, calcite; Chl, chlorite; Cpx, clinopyroxene; Dol, dolomite; Ep, epidote; Grt, garnet; Hbl, hornblende; Kfs, K-feldspar; Mag, magnetite; Mus, muscovite; Ol, olivine; Opq, opaque; Opx, orthopyroxene; Phl, phlogopite; Phn, phengite; Pl, plagioclase; Qtz, quartz; Rt, rutile; Srp, serpentine; Symp, symplectite; Tlc, talc; Zo, zoisite.
[b]The goodness of fit coefficients $R^2 > 0.98$ for all the samples.

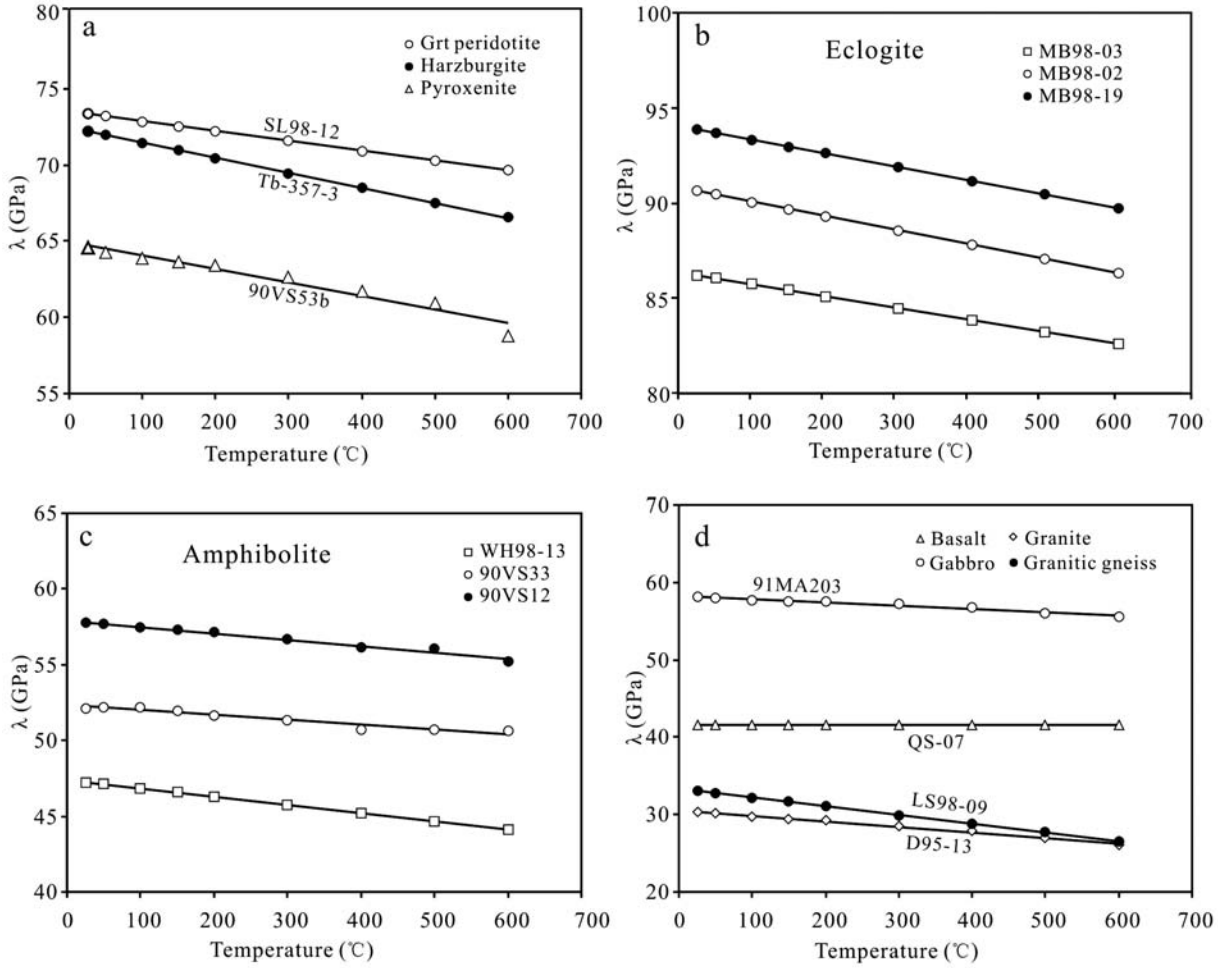

Figure 2. The effect of temperature on Lamé parameter for (a) harzburgite, garnet (Grt) peridotite and pyroxenite, (b) eclogites, (c) amphibolites, and (d) basalt, granite, granitic gneiss and gabbro at a hydrostatic pressure of 600 MPa. The original wave velocities and density data are from *Barruol* [1993], *Kern et al.* [1999], *Kern et al.* [2002], and *Kern and Tubia* [1993].

Table 2. Densities, Modal Compositions, and Parameters λ_0 and $d\lambda/dT$ Describing the Effect of Temperature for 13 Samples Shown in Figure 2

Sample	Lithology	Density (g/cm^3)	Modal Composition[a]	λ_0 (GPa)	$d\lambda/dT$ (GPa/°C)	R^2	Source of Data
90VS12	Amphibolite	3.14	Hbl 59.0, Pl 35.0, Qtz 4.0, Opq 1.0	57.92	0.0042	0.98	*Barruol* [1993]
90VS33	Amphibolite	3.07	Hbl 54.2, Pl 35.8, Pyx 8.0, Opq 2.0	52.32	0.0032	0.94	*Barruol* [1993]
QS-07	Basalt	2.74	Matrix 70.0, Pyx 19.0, Pl phenocryst 6.0, Idd 5.0	41.65	0.000005	0.81	*Kern et al.* [2002]
MB98-02	Eclogite	3.57	Grt 57.0, Omp 42.0, Rt 0.6, Mus 0.2	90.81	0.0075	0.99	*Kern et al.* [2002]
MB98-03	Eclogite	3.45	Grt 46.0, Omp 53.0, Mus 0.6	86.36	0.0062	0.99	*Kern et al.* [2002]
MB98-19	Eclogite	3.61	Grt 80.0, Omp 15.0, Phl 3.5, Qtz 1.0, Opq 0.5	94.05	0.0072	0.99	*Kern et al.* [2002]
91MA203	Gabbro	2.90	Pl 75.0, Opx 22.0, Hbl 2.0, Bt 1.0	58.23	0.0042	0.98	*Barruol* [1993]
D95-13	Granite	2.65	Pl 54.0, Kfs 23.0, Qtz 20.0, Bt 3.0	30.57	0.0071	0.99	*Kern et al.* [1999]
LS98-09	Granitic gneiss	2.64	Kfs 53.0, Qtz 29.0, Mus 6.0, Pl 8.0, Ep 4.0, Sp 0.2, Bt 0.1	33.33	0.0112	1.00	*Kern et al.* [2002]
WH98-13	Grt amphibolite	3.24	Hbl 65.0, Qtz 18.0, Grt 15.0, Mag 2.0, Pl 0.4	47.39	0.0054	0.99	*Kern et al.* [2002]
SL98-12	Grt peridotite	3.39	Ol 73.0, Mag 14.0, Grt 12.0, Pyx 1.0	73.5	0.0065	1.00	*Kern et al.* [2002]
Tb-357-3	Harzburgite	3.30	Ol 74.0, Opx 21.5, Cpx 2.5, Spl 1.6, Srp 0.4	72.42	0.0098	1.00	*Kern and Tubia* [1993]
90VS53b	Pyroxenite	3.24	Pyx 68.5, Pl 25.4, Spl 4.5, Opq 1.6	64.97	0.0089	0.96	*Barruol* [1993]

[a]Abbreviations are Bt, biotite; Cpx, clinopyroxene; Ep, epidote; Grt, garnet; Hbl, hornblende; Idd, iddingsite; Kfs, K-feldspar; Mag, magnetite; Mus, muscovite; Ol, olivine; Omp, omphacite; Opq, opaque; Opx, orthopyroxene; Phl, phlogopite; Pl, plagioclase; Pyx, proxene; Qtz, quartz; Rt, rutile; Srp, serpentine; Sp, sphalerite; Spl, spinel.

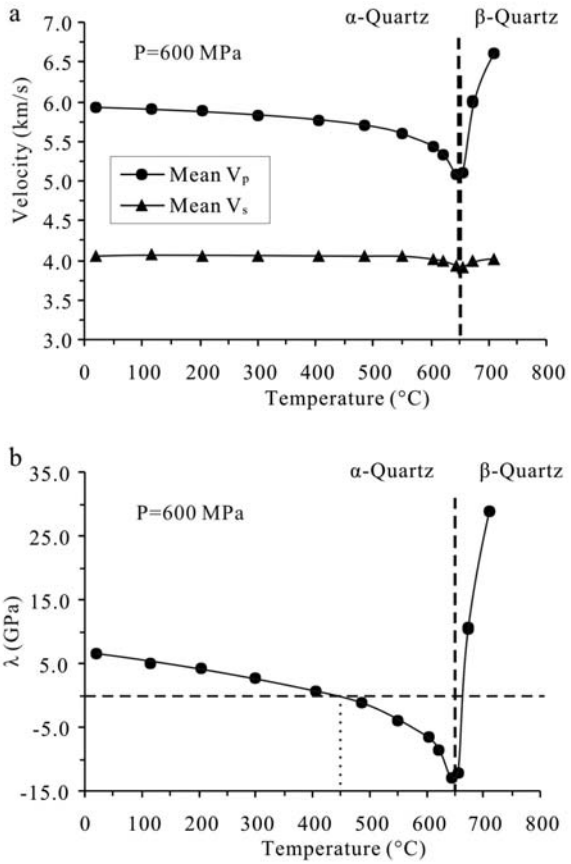

Figure 3. (a) Mean P and S wave velocities and (b) Lamé parameter as a function of temperature for a quartzite at a confining pressure of 600 MPa. The wave velocity data are from *Barruol* [1993]. The α-β quartz transition occurs at ~650°C.

Massif (northern Pyrenees, France), and its P and S wave velocities and densities were measured in three propagation directions (*X*, *Y*, *Z*) and six propagation-polarization directions (XY, XZ, YX, YZ, ZX and ZY), respectively [*Barruol*, 1993; *Barruol et al.*, 1992]. The P wave velocity falls pronouncedly when approaching the α-β quartz transition temperature (~650°C at 600 MPa), and jumps abruptly after the transition while little change occurs in the S wave velocity across the transition. A similar phenomenon was observed in other quasi-isotropic quartzites [*Kern*, 1979]. The λ values (Figure 3b) computed from the mean V_p, V_s, and density values for the quartzite become negative in the temperature range from 450°C to 650°C. An abrupt increase in λ occurs above 650°C at 600 MPa, reflecting a pronounced increase in V_p/V_s ratio in the beta quartz. Previous experiments [e.g., *Shen et al.*, 1993] showed that the α-β quartz transition temperature increases linearly with increasing the confining pressure. In the quartz-rich continental crust with an anomalously high geothermal gradient ($dT/dz > 25$ °C), one may expect to detect low, very low and high λ values for the upper crust (<450°C), middle crust (450–650°C) and lower crust (>650°C), respectively. In other words, as the α-β quartz transition is expected to occur in the quartz-bearing rocks (i.e., granite, diorite, and felsic gneiss) across the boundary between the middle and the lower crusts, a significant decrease in λ or υ may mark this boundary.

3.4. The λ-ρ Correlation

[15] Figure 4 shows fields of different types of rocks within the λ-ρ plots at a hydrostatic confining pressure of 600 MPa under which the effect of microcracks is eliminated. The field boundary contours were drawn by eye according to the distribution of experimental data. For peridotites, both λ and ρ values decrease progressively with increasing the content of serpentine (chrysotile, antigorite, and lizardite [*Watanabe et al.*, 2007]) (Figure 4a). This trend is consistent with the preliminary results of *Christensen* [1966] for ultramafic rocks. The field of peridotites is relatively large due to varying contents of garnet, spinel and magnetite, which have high values in both λ and ρ. For mafic rocks, eclogite displays significantly higher values of both λ and ρ than gabbro, diabase, mafic gneiss, mafic granulite and amphibolite. The large variations in both λ and ρ for eclogites are attributable to varying volume fractions of garnet, rutile and magnetite. Acid and intermediate rocks (i.e., granite, diorite, felsic gneiss, intermediate gneiss and metasediments) have lower λ and ρ values than the mafic crystalline rocks (Figure 4b). The fields for limestone/marble, anorthosite, and basalt are also identified in Figure 4c. As shown in Figure 5a, λ illustrates a clear trend of linear increase with density. The best fitting of the data for 401 samples gives: $\lambda = 57.814\,\rho - 118.51$ ($R^2 = 0.79$), λ is in GPa, and ρ is in g/cm^3. In the statistical analysis, porous (basalt and sandstone) and hydrated (serpentinite) rocks are not included. There is considerable scatter is the distribution of the λ-ρ data for peridotites and eclogites due to mineralogical complexities (mainly the content of garnet). This will be analyzed in more detail in the Discussion.

3.5. The λ-V_p Correlation

[16] Figure 6 provides λ-V_p plots for different categories of rocks at a confining pressure of 600 MPa. The trend of λ variation with V_p for peridotites with various degrees of serpentinization reflects essentially progressive decreases in both λ and V_p with increasing the content of serpentine (Figure 6a). It is noted that the presence of garnet, spinel or chromite may cause a significant increase in λ for peridotites. Eclogite displays higher values of both λ and V_p than the other mafic rocks such as gabbro, diabase, mafic gneiss, mafic granulite and amphibolite. Acid and intermediate rocks such as granite, diorite, felsic gneiss, intermediate gneiss and metasediments have lower λ and V_p values (Figure 6b). Limestones/marbles show intermediate λ and V_p values between anorthosite and sandstone (Figure 6c). The best fitting of the data for 401 samples (except of basalt, sandstone and serpentinite) gives: $\lambda = 25.775 V_p - 125.84$ ($R^2 = 0.90$), where λ is in GPa, and V_p is in km/s (Figure 5b).

3.6. The λ-V_s Correlation

[17] Variations of λ values as a function of V_s are shown in Figure 7 for different groups of rocks at a hydrostatic confining pressure of 600 MPa. Fresh peridotites can be clearly distinguished from serpentinite and partially serpentinized peridotites in the λ- V_s diagram (Figure 7a). Eclogite can be easily separated from the other mafic rocks such as gabbro, diabase, mafic gneiss and mafic granulite

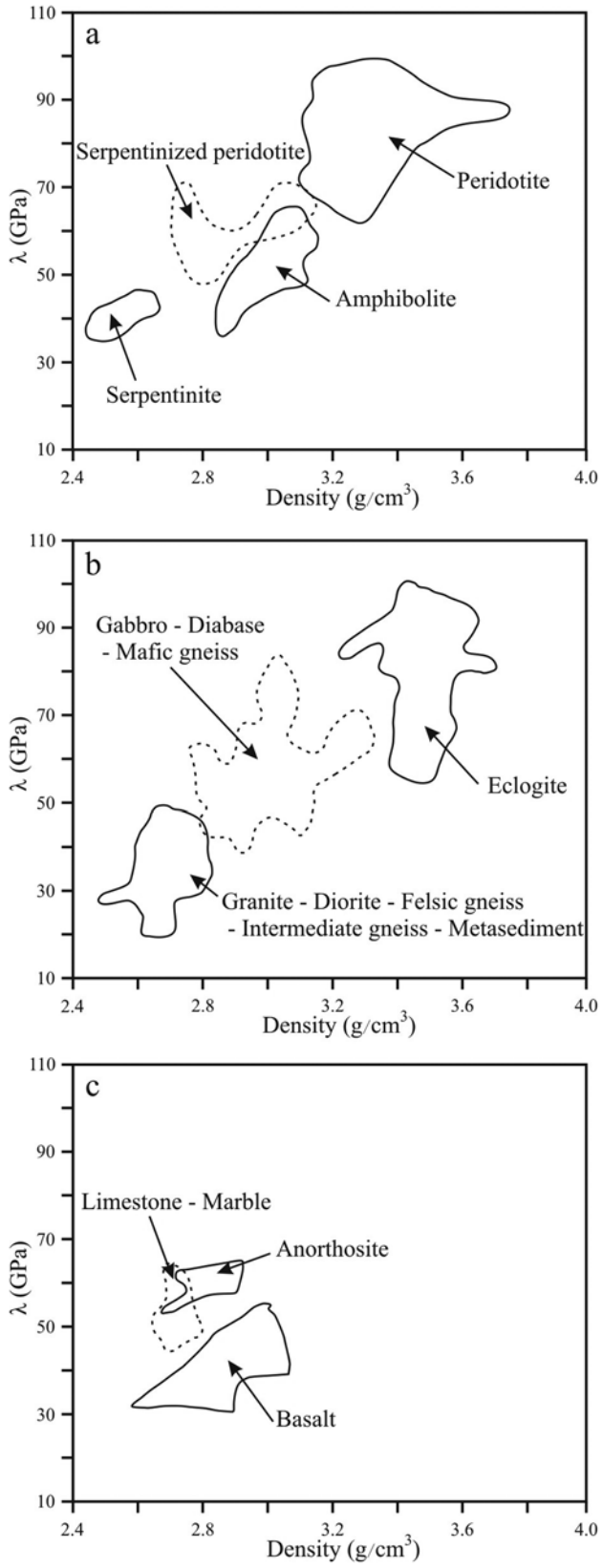

Figure 4. The λ-ρ plots for (a) 31 amphibolites, 38 peridotites, 12 serpentinites, and 15 partially serpentinized peridotites, (b) 54 eclogites, 118 mafic rocks (gabbro, diabase, mafic gneiss and mafic granulite) and 145 felsic rocks (granite, diorite, felsic gneiss, intermediate gneiss, and metasediments), and (c) 8 anorthosites, 21 basalts, and 29 limestones/marbles at a hydrostatic pressure of 600 MPa.

according to their λ-V_s plots. Felsic rocks including granite, diorite, felsic gneiss, intermediate gneiss and metasediments are characterized by relatively lower λ values (Figure 7b). Important differences between Figure 6b and Figure 7b originate from the high V_s value of quartz, which affects the relative positions of quartz-rich rocks (e.g., granite, granodiorite, diorite, and felsic gneiss). Porous volcanic basalts show significantly lower values in both λ and V_s than calcite-rich limestone-marble and plagioclase-rich anorthosite (Figure 7c). The best fitting of the data from 401 samples (excluding basalt, sandstone, and serpentinite) yields: $\lambda = 40.122V_s - 104.34$ ($R^2 = 0.62$), where λ is in GPa, and V_s in km/s (Figure 5c). Obviously, the correlation of λ with V_p (Figure 5b) is remarkably better than that with V_s (Figure 5c).

3.7. The μ-λ Correlation

[18] It is interesting to plot μ as a function of λ because these two invariants form the basic elements within all the elastic properties. If different types of rocks tend to separate from each other in the μ-λ diagram, these two parameters may be used as a discriminant of lithological compositions. As shown in Figure 8, fresh peridotites, serpentinites and partially serpentinized peridotites can be distinguished each other in the μ-λ plot. The ultramafic rocks display systematic decreases in both μ and λ with increasing the degree of serpentinization. The parameter λ is always larger than μ with the mean μ/λ ratios equal to 0.810, 0.641 and 0.460 for the peridotite (38 samples), serpentinized peridotite (15 samples) and serpentinite (12 samples), respectively. The ratios correspond to the mean Poisson's ratios of 0.275, 0.305 and 0.343 for the peridotite, serpentinized peridotite and serpentinite, respectively. In Figure 8a, amphibolites (31 samples) deviate clearly from the trend of the ultramafic rocks. According to the μ-λ plot, eclogite can be separated from the other mafic rocks (e.g., gabbro, diabase, amphibolite, mafic gneiss and mafic granulite) as well as felsic rocks (e.g., granite, diorite, felsic gneiss, intermediate gneiss, and metasediments). The mean μ/λ ratios are 0.818, 0.915 and 1.057, corresponding to the mean Poisson's ratios of 0.275, 0.261 and 0.243, for the mafic rocks (118 samples), eclogites (54 samples), and felsic rocks (145 samples), respectively. Eclogite exhibits remarkably higher values of both μ and λ than the other common mafic rocks such as gabbro, diabase, mafic gneiss, mafic granulite and amphibolite. Data of acid and intermediate rocks (e.g., granite, diorite, felsic gneiss, intermediate gneiss and metasediments) cluster in a small area with lower μ and λ values. Limestone/marble (29 samples), basalt (21 samples), and anorthosite (8 samples) can also be separated from each other in the μ-λ plots (Figure 8c).

[19] For reservoir sedimentary rocks that are generally porous, *Goodway et al.* [1997] and *Gray and Andersen* [2000] used a cross plot of $\mu\rho$ versus $\lambda\rho$ in place of a

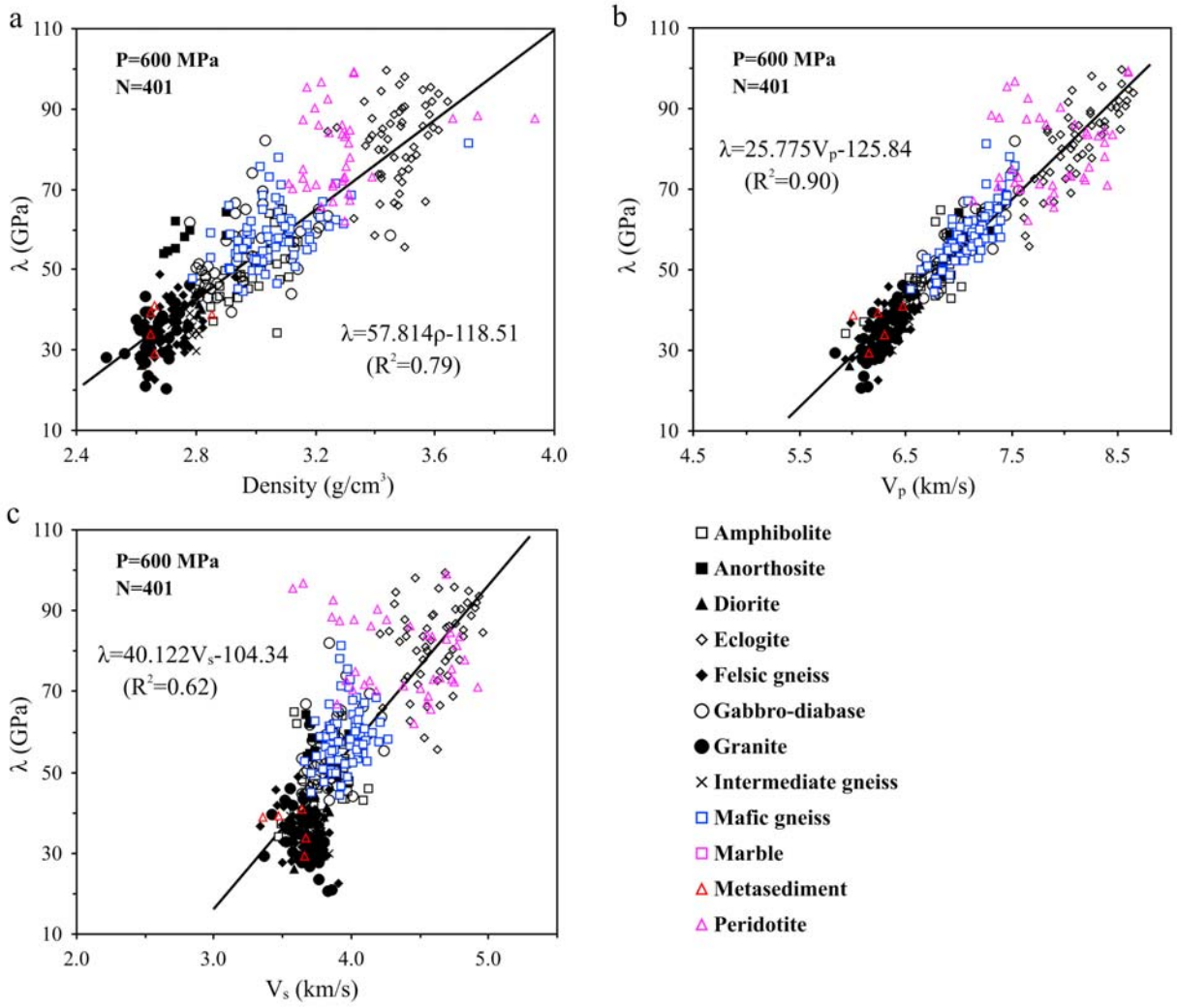

Figure 5. Variations in Lamé parameter (λ) with (a) density, (b) V_p, and (c) V_s for various types of rocks at a hydrostatic pressure of 600 MPa for 401 samples. Serpentinite and porous rocks such as basalt and limestone are not included.

μ-λ diagram. According to these authors, different types of lithology tend to separate along orthogonal boundaries in such a $\mu\rho - \lambda\rho$ cross plot: (1) coals have the lowest values of both $\lambda\rho$ and $\mu\rho$. (2) Carbonates have high values of both $\lambda\rho$ and $\mu\rho$. (3) Gas-filled sandstones have low $\lambda\rho$ values but high $\mu\rho$ values. A combination of $\lambda\rho$ and $\mu\rho$ values has been used for quick determination of reservoir lithology and gas content [e.g., *Li et al.*, 2003].

4. Discussion

[20] In this section, we analyze the relationship between λ and mineral composition of the crystalline rocks (Figures 4–8). Figures 9a and 9b, plotting λ versus ρ and μ versus λ, respectively, provide some interesting perspectives on λ characteristics of pure monomineralic aggregates of common rock-forming minerals. The λ value of a polymineralic composite rock depends presumably on the volume fractions and the λ values of its constituent minerals. The contribution of each constituent mineral to the bulk λ value of a composite rock can be analyzed for the moment only in a qualitative manner because a relevant mixture rule for λ is not available [*Lubarda*, 1998; *Nadeau*, 1999; *Berryman*, 1995; *Ji and Xia*, 2002; *Ji*, 2004; *Mavko et al.*, 2009]. The utilization of the λ-ρ and μ-λ plots for lithological discrimination is also discussed.

[21] Quartz is characterized by extremely low values in both λ (~8.1 GPa) and ρ (2.65 g/cm^3) but moderate value in μ (44.4 GPa) [*Bass*, 1995]. Hence, it lies obviously below and above the general trends in the λ-ρ (Figure 9a) and μ-λ (Figure 9b) diagrams, respectively. Moreover, quartz-rich sandstones should have significantly lower λ or $\lambda\rho$ values than calcite-rich or dolomite-dominant carbonates. This feature can be used for quick determination of reservoir lithology and in turn is economically important for oil or gas field exploration in sedimentary basins [*Goodway et al.*, 1997; *Goodway*, 2001; *Gray and Andersen*, 2000; *Gray*, 2003; *Dufour et al.*, 2002]. In the seismological investigation of carbonate reservoir in the Western Canadian sedimentary basin [*Goodway et al.*, 1997; *Li et al.*, 2003], for example, $\lambda\rho$ and μ/λ were used as a good indicator for distinguishing tight limestone ($\lambda\rho$ = ~90.0 GPa g/cm^3 and μ/λ = ~0.81), wet dolomite ($\lambda\rho$ =~75.0 GPa g/cm^3, μ/λ =

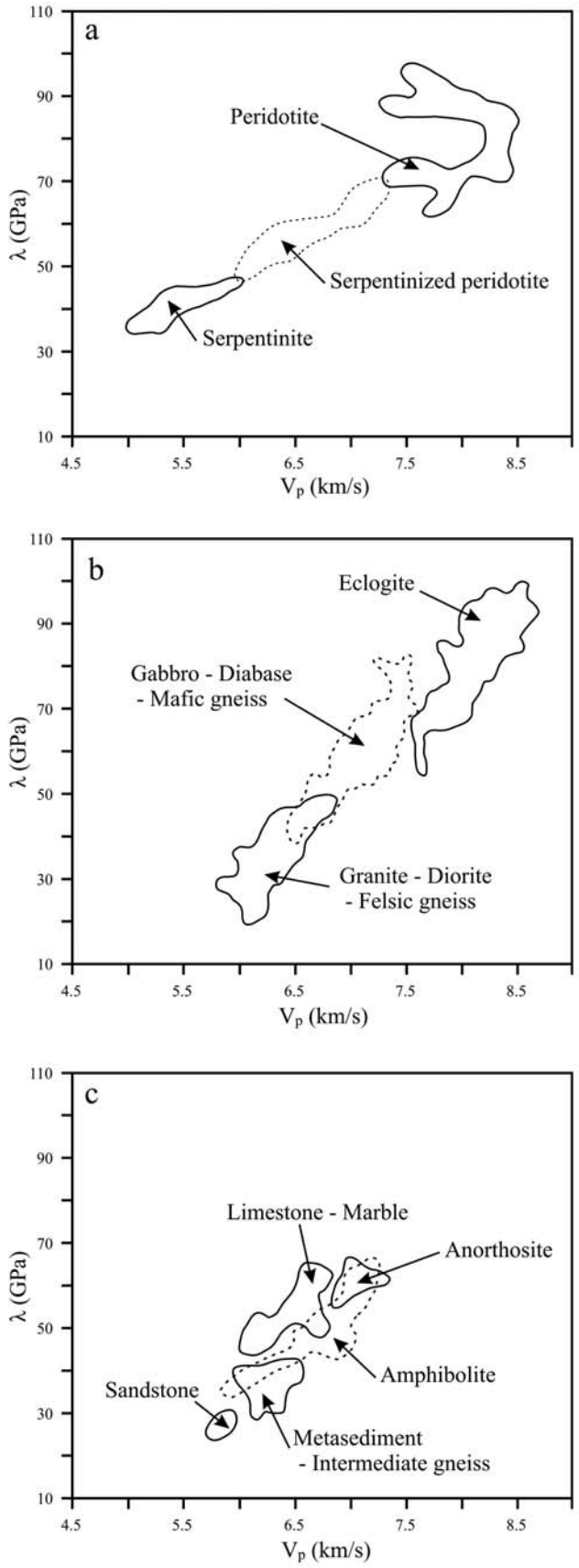

Figure 6. The λ-V_p plots for (a) 38 peridotites, 12 serpentinites, and 15 partially serpentinized peridotites, (b) 54 eclogites, 118 mafic rocks (gabbro, diabase, mafic gneiss and mafic granulite) and 145 felsic rocks (granite, diorite, felsic gneiss, intermediate gneiss, and metasediments), and (c) 31 amphibolites, 8 anorthosites, 21 basalts, and 29 limestones/marbles at a hydrostatic pressure of 600 MPa.

~1.24) and gas dolomite ($\lambda\rho$ =~37.5 GPa g/cm^3, μ/λ = ~2.08). The gas effect is apparent on reducing the $\lambda\rho$ and μ/λ values because the presence of gas in porous, grain-supported rocks causes a significant decrease in its incompressibility (K) but does not affect its rigidity (μ). As a result, λ is significantly reduced by the presence of gas. In petroleum industry, therefore, layers of low λ or $\lambda\rho$ values derived from the inversion of amplitude versus offset (AVO) stacks often suggest the presence of gas in a sandstone or dolomite reservoir [*Goodway and Tessman*, 2000; *Gray and Andersen*, 2000]. In addition, coals have low rigidity and thus low shear modulus, and have low incompressibility and hence low λ values.

[22] Feldspars, which are the most abundant minerals in the Earth's crust, form a ternary system of three end-members: $KAlSi_3O_8$ (orthoclase), $NaAlSi_3O_8$ (albite) and $CaAl_2Si_2O_8$ (anorthite). For the plagioclase series, λ, μ and ρ all increase nearly linearly with increasing the amount of anorthite component (Figure 9). There is a nearly linear relationship between λ and ρ or between μ and λ for plagioclase feldspars. The alkali feldspars have lower λ and μ values than plagioclase feldspars. Nepheline (Ne) and serpentine (Srp) lie at almost the same position as orthoclase (Or) in the λ-ρ diagram, although these three minerals are separated in the μ-λ diagram with $\mu_{Ne} > \mu_{Or} > \mu_{Srp}$. In either the λ-ρ or μ-λ diagram (Figure 9), both alkali and plagioclase feldspars can be clearly separated from quartz. Thus, the λ-ρ and μ-λ plots may be used to discriminate quartz-from feldspar-dominant layers or domains in the continental crust. Furthermore, Figure 9 illustrates the reason why acid and intermediate rocks (e.g., granite, diorite, felsic gneiss, intermediate gneiss and metasediments), which consist of alkali feldspar, plagioclase, quartz, and mica, are low in both λ and ρ or μ and λ values.

[23] Accessory minerals such as zircon, rutile, ilmenite, sillimanite and spinel show generally very high λ and μ values with respect to the main rock-forming silicate minerals (Figure 9). Increasing the content of these minerals will result in an increase of λ and μ for the bulk rock.

[24] In the μ-λ diagram (Figure 9b), pyroxenes (ferrosilite, augite, diallage, bronzite, enstatite, diopside, hedenbergite, and aegirine) form a lozenge-shaped domain while high pressure pyroxenes, omphacite, and jadeite, lie at far outside this domain. Compared with jadeite and omphacite, diallage, enstatite, bronzite, and augite have relatively lower λ values. Ferrosilite has a much higher density than diopside, but both minerals show similar λ values. The role of Fe-Mg substitution in orthopyroxenes can be seen by the comparison between enstatite ($MgSiO_3$) and ferrosilite ($FeSiO_3$): ρ = 3.198 g/cm^3, μ = 75.7 GPa, λ = 57.3 GPa, and μ/λ = 1.32 for enstatite whereas ρ = 4.002 g/cm^3, μ = 52.0 GPa, λ = 66.3 GPa, and μ/λ = 0.78 for ferrosilite. Hornblende shows similar λ and ρ values to enstatite. In the μ-λ diagram,

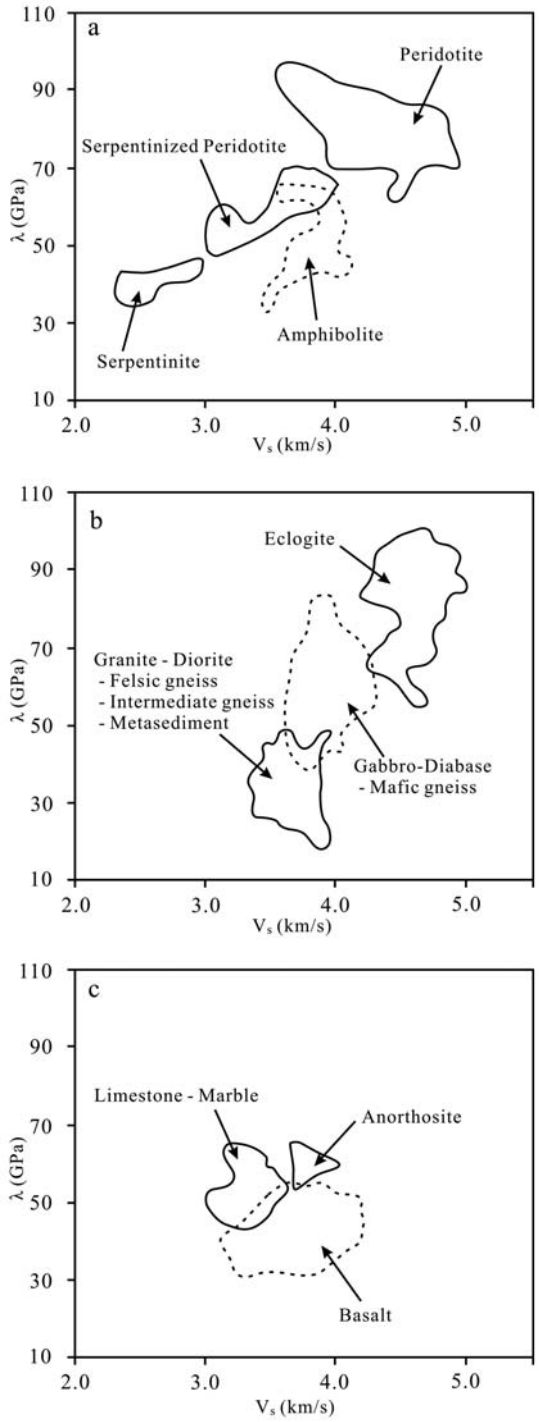

Figure 7. The λ-V_s plots for (a) 31 amphibolites, 38 peridotites, 12 serpentinites and 15 partially serpentinized peridotites, (b) 54 eclogites, 118 mafic rocks (gabbro, diabase, mafic gneiss, and mafic granulite) and 145 felsic rocks (granite, diorite, felsic gneiss, intermediate gneiss, and metasediments), and (c) 8 anorthosites, 21 basalts, and 29 limestones/marbles at a hydrostatic pressure of 600 MPa.

however, hornblende lies close to anorthite. Obviously, mafic rocks (e.g., gabbro, diabase, mafic gneiss and mafic granulite) in which pyroxene and labradorite-rich plagioclase (50% to 70% anorthite) are principal constituents have moderate μ, λ and ρ values between the end-members.

[25] In the olivine group [$(Fe, Mg)_2SiO_4$], both λ and ρ values increases with increasing the content of Fe_2SiO_4 (fayalite) whereas the μ value increases with increasing the content of Mg_2SiO_4 (forsterite). In other words, λ shows a positive correlation with ρ, but a negative correlation with μ for olivine. The role of Fe-Mg substitution in olivines is particularly significant: $\rho = 3.222$ g/cm^3, $\mu = 81.7$ GPa, $\lambda = 74.2$ GPa, and $\mu/\lambda = 1.1$ for forsterite whereas $\rho = 4.377$ g/cm^3, $\mu = 50.8$ GPa, $\lambda = 102.7$ GPa, and $\mu/\lambda = 0.49$ for fayalite. Figure 9 also indicates the position of olivine with forsterite contents Fo100 to Fo90, which represents the typical composition of common olivine in the upper mantle. In both the λ-ρ and μ-λ diagrams, the upper mantle olivine is located close to omphacite. A peridotite which is a mixture of olivine, orthopyroxene and clinopyroxene should lie somewhere among these three end-members, and the exact position depends on the volume fraction of each constituent and also on the amount of accessory minerals such as spinel, garnet, magnetite and ilmenite. The μ, λ and ρ of peridotites decrease with increasing the degree of serpentinization because serpentine as their hydrated product has extremely low values in λ (32.3 GPa), μ (15.67 GPa) and ρ (2.516 g/cm^3). Thus, the λ or $\lambda\rho$ data may allow the prediction of the serpentine content in the oceanic lithosphere from the inversion of surface seismic data through AVO methods.

[26] In the λ-ρ or μ-λ diagram (Figure 9), silicate garnets can be classified into two groups: pyralspite (pyrope-almandine-spessartine) and ugrandite (uvarovite-grassular-andradite) groups. From pyrope to almandine or spessartine, λ remains almost unchanged, but ρ increases considerably. The μ and λ values for pyrope, almandine and spessartine are very similar (Figure 9b). Therefore differences in the relative proportions of these components have little influence on the μ and λ values of pyralspite. Uvarovite displays higher λ values than andradite although they have similar densities. From grossular to andradite, λ increases slightly but ρ increases and μ decreases significantly (Figure 9).

[27] Eclogites, which consist of garnet and omphacite with rutile and magnetite as accessory minerals, are certainly very high in μ, λ and ρ values (Figures 4 and 8). The mafic granulite-eclogite transformation occurs near the base of thickened continental crust that is forced into the upper mantle during a collisional orogeny. Such a huge mass of eclogite may delaminate from the crust and sink into the mantle. As indicated by Figures 4b and 8b, the transition from mafic granulite or gabbro to eclogite should result in a significant increase in λ, μ and ρ. Such striking contrasts make distinction between eclogite and mafic granulite possible. Eclogite has seismic velocities similar to surrounding mantle peridotite (Figures 5b and 5c). However, the distinction of eclogite from peridotite is likely in the λ-ρ diagram (Figure 5a).

[28] Muscovite shows a relatively lower λ value with respect to its density (Figure 9). If the similar situation is true for other phyllitic minerals (e.g., biotite, phengite, phlogopite and chlorite) whose elastic constants are not available due to experimental restrictions, one would expect that the mica-rich rocks, which often occur in retrograde

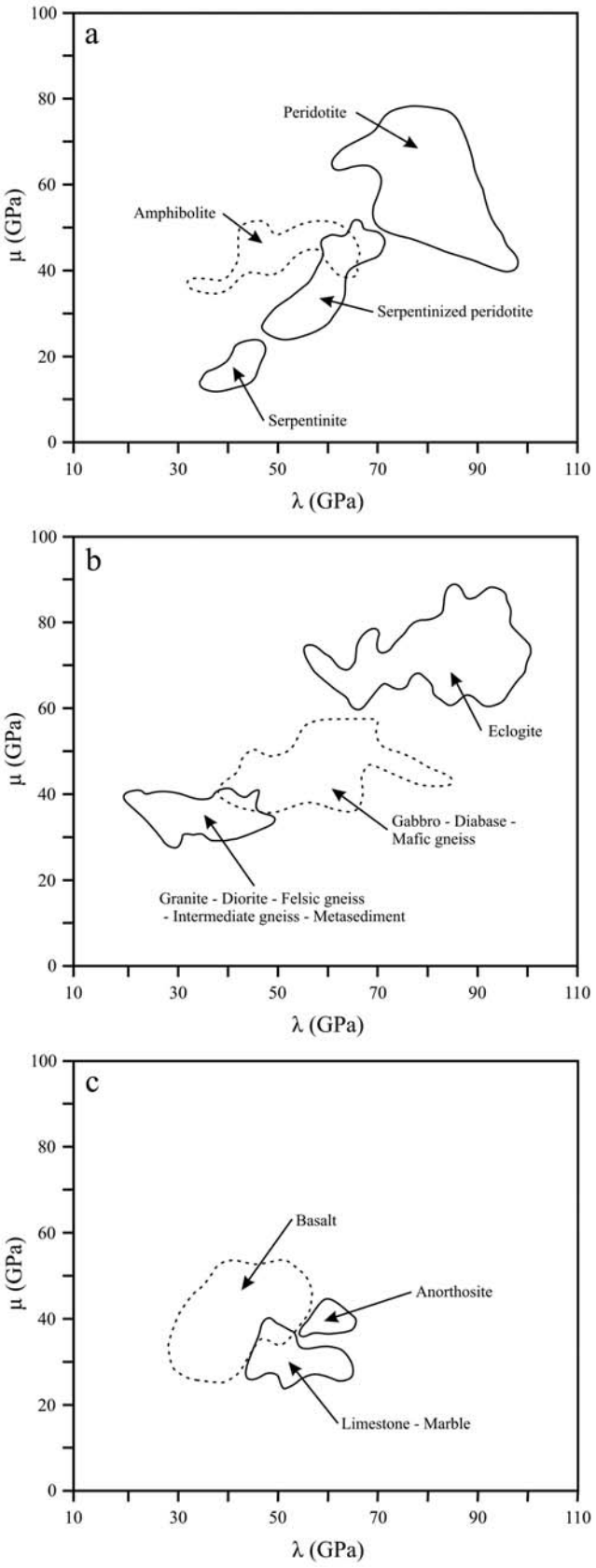

shear zones within the continental crust, are characterized by low λ values.

[29] As illustrated in Figure 8, the variation range in either μ or λ is much larger for mafic rocks than high-silica rocks. These differences reflect the fact that there is considerable variation in plagioclase, clinopyroxene, orthopyroxene, hornblende, and garnet in mafic rocks of various origins (magmatic crystallization for gabbro and diabase, and metamorphism for mafic granulite and mafic gneiss). Both the μ and λ values of these minerals are very disparate and hence a change in their relative proportion has a significant effect on these elastic parameters. In the felsic rocks, however, the dominant minerals are potassium feldspar and sodic plagioclase, both having similar μ and λ values. Thus variations in μ and λ correspond mainly to the difference in the relative proportion of quartz in the felsic rocks. Similarly, the large range of variations in μ and λ values for eclogites result principally from the difference in the relative proportion of garnet.

[30] Metamorphism is also an important factor to influence the λ value of a rock. For example, pelitic rocks at greenschist facies grades contain chlorite, muscovite, quartz and albite. At the upper amphibolite or granulite facies grades, however, the rocks with the same chemical composition contain garnet, sillimanite, oligoclase or andesine, quartz and hornblende or pyroxene [*Burlini and Fountain*, 1993]. Increases in the contents of garnet, sillimanite, hornblende and pyroxene and in anorthite content of plagioclase during progressive metamorphism should systematically result in an increase in rock's λ value.

[31] Finally, the presence of fluids in porous materials such as sedimentary rocks affects significantly λ but not μ [*Goodway*, 2001]. The parameters μ and λ are sensitive to the rock matrix and pore fluids, respectively. For example, it is impossible to distinguish shale (V_p = 2.898 km/s) from gas sandstone (V_p = 2.857 km/s) according their P wave velocities. However, it is easy to discriminate these rocks according to their λ values: 12.3 GPa for shale and 5.9 GPa for gas sandstone. The reason is simple. As $V_p = \sqrt{(\lambda + 2\mu)/\rho}$, the λ decrease of sandstone due to the gas porosity is nearly completely offset by an increase in 2μ resulting from the predominance of quartz in sandstone over shale.

5. Conclusion

[32] Lamé parameter (λ), which is closely related to the incompressibility and contains a high proportion of information about the resistance to a change in volume caused by a change in pressure, is an important, intrinsic, elastic property of rocks. Only λ and shear modulus (μ) appear in Hooke's law and not Young's modulus (E), the bulk modulus (K) or Poisson's ratio (υ). Unfortunately, so far little

Figure 8. The μ-λ plots for (a) 31 amphibolites, 38 peridotites, 12 serpentinites and 15 partially serpentinized peridotites, (b) 54 eclogites, 118 mafic rocks (gabbro, diabase, mafic gneiss, and mafic granulite) and 145 felsic rocks (granite, diorite, felsic gneiss, intermediate gneiss, and metasediments), and (c) 8 anorthosites, 21 basalts, and 29 limestones/marbles (c) at a hydrostatic pressure of 600 MPa.

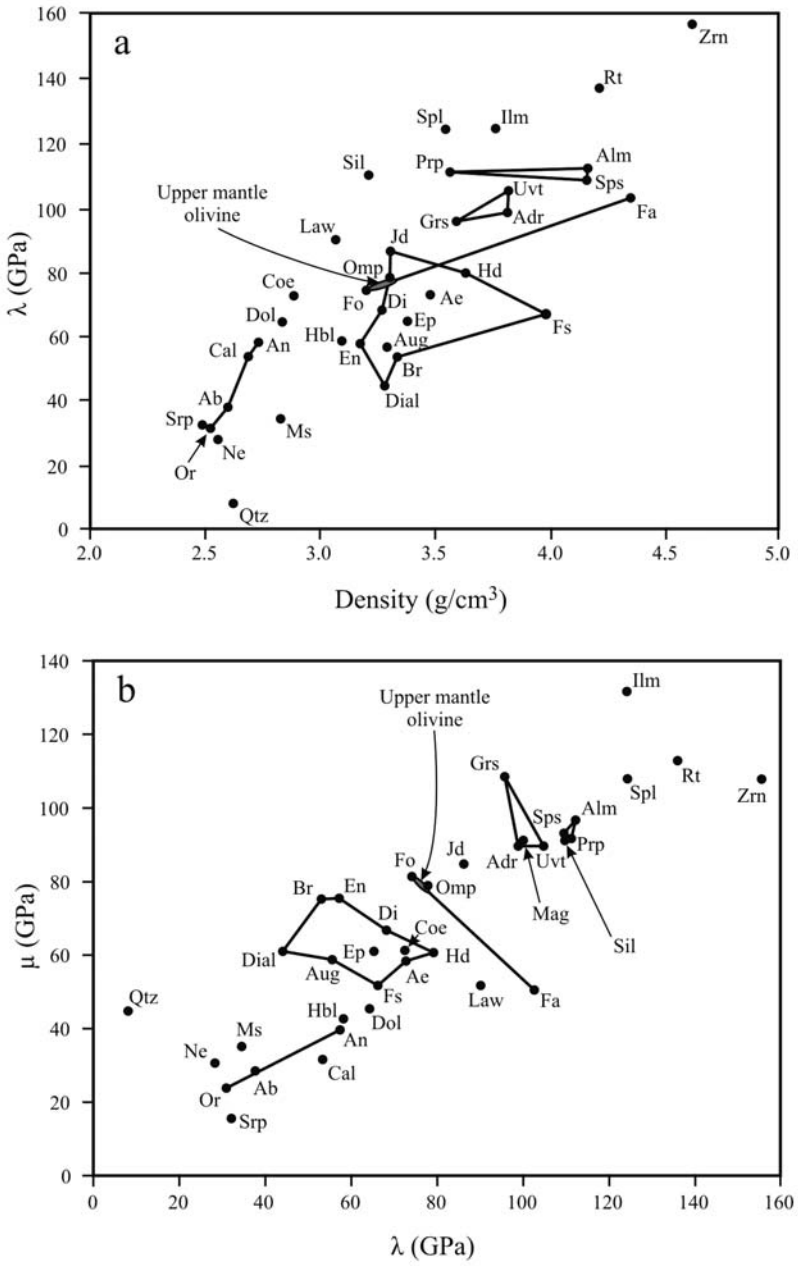

Figure 9. The (a) λ-ρ and (b) μ-λ plots for main rock-forming minerals. Ab, albite; Adr, andradite; Ab, albite; Adr, andradite; Ae, aegirine; Alm, almandine; An, anorthite; Aug, augite; Br, bronzite; Cal, calcite; Coe, coesite; Di, diopside; Dial, diallage; Dol, dolomite; En, enstatite; Ep, epidote; Fa, fayalite; Fo, forsterite; Fs, ferrosilite; Grs, grossular; Hbl, hornblende; Hd, hedenbergite; Ilm, ilmenite; Jd, jadeite; Law, lawsonite; Mag, magnetite; Ms, muscovite; Ne, nepheline; Omp, omphacite; Or, orthoclase; Prp, pyrope; Qtz, quartz; Rt, rutile; Sil, sillimanite; Spl, spinel; Sps, spessartine; Srp, serpentine; Uvt, uvarovite; Zrn, zircon. The values of λ and μ for each mineral were calculated from the elastic constants compiled by *Bass* [1995].

has been known about the characteristic λ value for each common type of crystalline rocks that constitute the Earth's crust and upper mantle and its variation with pressure (P), temperature (T) and mineralogical composition. Here we fill such a gap by analyzing in details the λ values of 475 natural rocks on which mean P and S wave velocities have been measured at high hydrostatic pressures (≥400 MPa) using the same laboratory equipment and the same method. The λ value of an equivalent isotropic crystalline rock as a function of confining pressure (P) and temperature (T) can be described by $\lambda = a + (d\lambda/dP)P - c\exp(-kP) - (d\lambda/dT)T$, where a is the projected λ value at zero pressure if microcracks were fully closed; $d\lambda/dP$ is the pressure derivative in the linear elastic regime; c is the initial λ drop caused by the presence of microcracks at zero pressure; k is a decay constant of the λ drop in the nonlinear poroelastic regime;

and $d\lambda/dT$ is the temperature derivative. The laboratory experimental data may be extrapolated to the Earth's interior using the above equation if no partial melting, metamorphic reaction, dehydration or phase transformation occurs. In the λ-ρ and μ-ρ plots, the main categories of lithology can be clearly discriminated. The ultramafic rocks display systematic decreases in both μ and λ with increasing the degree of serpentinization. Eclogites, mafic rocks (gabbro, diabase, mafic granulite, and mafic gneiss) and felsic rocks (granite, diorite, felsic gneiss, intermediate gneiss and metasediments) are characterized by high, moderate and low μ and λ values, respectively. For pyroxenes and olivines, both λ and ρ increase but μ decreases with increasing the Fe/Mg ratios. In the plagioclase series, both λ and μ increases with increasing the anorthite content. Increases in the contents of garnets, sillimanite, rutile, zircon, ilmenite and spinel result systematically in an increase in rock's λ and μ values. The results suggest that the λ-ρ and μ-ρ plots can be used as a discriminant of composition for rocks in the Earth's crust and upper mantle. This is particularly important because the connection between composition and seismic P or S wave velocity is not unique due to similar velocities of many common rock types.

[33] **Acknowledgments.** S. Ji thanks the Natural Sciences and Engineering Council of Canada for the discovery grants and the Chinese Academy of Geological Sciences for research grants. Qian Wang was supported by the knowledge Innovation Program from Guangzhou Institute of Geochemistry, Chinese Academy of Sciences (GIGCX-09-02).

References

Barruol, G. (1993), Pétrophysique de la croûte inférieure, Rôle de l'anisotropie sismique sur la réflectivité et le déphasage des ondes S, Ph.D. thesis, pp. 239–258, Univ. de Montpellier II, Montpellier, France.

Barruol, G., D. Mainprice, H. Kern, M. Saint Blanquat, and P. Compte (1992), 3D seismic study of a ductile shear zone from laboratory and petrofabric data (Saint Barthélémy Massif, northern Pyrénées, France), *Terra Nova*, *4*, 63–76, doi:10.1111/j.1365-3121.1992.tb00451.x.

Bass, J. D. (1995), Elasticity of minerals, glasses, and melts, in *Mineral Physics and Crystallography: A Handbook of Physical Constants*, *AGU Ref. Shelf*, vol. 2, edited by T. J. Ahrens, pp. 45–63, AGU, Washington, D. C.

Berryman, J. G. (1995), Mixture theories for rock properties, in *Rock Physics and Phase Relations: A Handbook of Physics Constants*, *AGU Ref. Shelf*, vol. 3, edited by T. J. Ahrens, pp. 205–228, AGU, Washington, D. C.

Birch, F. (1960), The velocity of compressional waves in rocks to 10 kilobar, Part 1, *J. Geophys. Res.*, *65*, 1083–1102, doi:10.1029/JZ065i004p01083.

Burke, M. M., and D. F. Fountain (1990), Seismic properties of rocks from an exposure of extended continental crust-new laboratory measurements from the Ivrea Zone, *Tectonophysics*, *182*, 119–146, doi:10.1016/0040-1951(90)90346-A.

Burlini, L., and D. M. Fountain (1993), Seismic anisotropy of metapelites from the Ivrea-Verbano zone and Serie dei Laghi (northern Italy), *Phys. Earth Planet. Inter.*, *78*, 301–317, doi:10.1016/0031-9201(93)90162-3.

Chávez-Pérez, S., and J. N. Louie (1997), Isotropic scattering and seismic imaging of crust fault zones using earthquakes, paper presented at 67th Annual International Meeting, Soc. of Explor. Geophys., Dallas, Tex.

Chávez-Pérez, S., and J. N. Louie (1998), Crustal imaging in southern California using earthquake sequences, *Tectonophysics*, *286*, 223–236, doi:10.1016/S0040-1951(97)00267-9.

Christensen, N. I. (1966), Elasticity of ultrabasic rocks, *J. Geophys. Res.*, *71*, 5921–5931.

Christensen, N. I. (1974), Compressional wave velocities in possible mantle rocks to pressures of 30 kilobars, *J. Geophys. Res.*, *79*, 407–412, doi:10.1029/JB079i002p00407.

Christensen, N. I., and R. Ramananantoandro (1971), Elastic moduli and anisotropy of dunite to 10 kilobars, *J. Geophys. Res.*, *76*, 4003–4010, doi:10.1029/JB076i017p04003.

Dufour, J., J. Squires, W. N. Goodway, A. Edmunds, and I. Shook (2002), Integrated geological and geophysical interpretation case study, and Lamé rock parameter extractions using AVO analysis on the Blackfoot 3C–3D seismic data, southern Alberta, Canada, *Geophysics*, *67*, 27–37, doi:10.1190/1.1451319.

Eberhart-Phillips, D., D. Han, and M. D. Zoback (1989), Empirical relationships among seismic velocity, effective pressure, porosity, and clay content in sandstone, *Geophysics*, *54*, 82–89, doi:10.1190/1.1442580.

Estabrook, C. H., and R. Kind (1996), The nature of the 660-kilometer upper-mantle seismic discontinuity from precursors to the PP phase, *Science*, *274*, 1179–1182, doi:10.1126/science.274.5290.1179.

Goodway, B. (2001), AVO and Lamé constants for rock parameterization and fluid detection, *CSEG Rec.*, *26*, 39–60.

Goodway, B., and J. Tessman (2000), Comparative reservoir imaging using new seismic-acquisition technology, *World Oil*, *221*, 49–54.

Goodway, B., T. Chen, and J. Downton (1997), Improved AVO fluid detection and lithology discrimination using Lamé petrophysical parameters, $\lambda\rho$, $\mu\rho$, and λ/μ fluid stack, from P and S inversions, paper presented at 67th Annual International Meeting, Soc. of Explor. Geophys., Dallas, Tex.

Gray, D. (2003), A better way to extract fundamental rock properties with much less noise, *World Oil*, *224*, 49–53.

Gray, D., and E. Andersen (2000), The application of AVO and inversion to formation properties, *World Oil*, *221*, 85–90.

Jaeger, J. C. (1969), *Elasticity, Fracture and Flow, With Engineering and Geological Applications*, 268 pp., Methuen, London.

Ji, S. C. (2004), A generalized mixture rule for estimating the viscosity of solid-liquid suspensions and mechanical properties of polyphase rocks and composite materials, *J. Geophys. Res.*, *109*, B10207, doi:10.1029/2004JB003124.

Ji, S. C., and M. H. Salisbury (1993), Shear-wave velocities, anisotropy and splitting in the high grade mylonites, *Tectonophysics*, *221*, 453–473, doi:10.1016/0040-1951(93)90173-H.

Ji, S. C., and B. Xia (2002), *Rheology of Polyphase Earth Materials*, 259 pp., Polytech. Int. Press, Montreal, Que., Canada.

Ji, S. C., and Z. Q. Xu (Eds.) (2009), The Chinese Continental Scientific Drilling (CCSD), *Tectonophysics*, *475*(2), 201–203, doi:10.1016/j.tecto.2009.04.007.

Ji, S. C., M. H. Salisbury, and S. Hanmer (1993), Petrofabric, P wave anisotropy and seismic reflectivity of high-grade tectonites, *Tectonophysics*, *222*, 195–226, doi:10.1016/0040-1951(93)90049-P.

Ji, S. C., Q. Wang, and B. Xia (2002), *Handbook of Seismic Properties of Minerals, Rocks and Ores*, 630 pp., Polytech. Int. Press, Montreal, Que., Canada.

Ji, S. C., K. Saruwatari, D. Mainprice, R. Wirth, Z. Q. Xu, and B. Xia (2003), Microstructures, petrofabrics and seismic properties of ultrahigh-pressure eclogites from Sulu region, China: Implications for rheology of subducted continental crust and origin of mantle reflections, *Tectonophysics*, *370*, 49–76, doi:10.1016/S0040-1951(03)00177-X.

Ji, S. C., Q. Wang, D. Marcotte, M. H. Salisbury, and Z. Q. Xu (2007), P wave velocities, anisotropy and hysteresis in ultrahigh-pressure metamorphic rocks as a function of confining pressure, *J. Geophys. Res.*, *112*, B09204, doi:10.1029/2006JB004867.

Ji, S. C., Q. Wang, and M. H. Salisbury (2009), Composition and tectonic evolution of the Chinese continental crust constrained by Poisson's ratio, *Tectonophysics*, *463*, 15–30, doi:10.1016/j.tecto.2008.09.007.

Kern, H. (1979), Effect of high-low quartz transition on compressional and shear wave velocities in rocks under high pressure, *Phys. Chem. Miner.*, *4*, 161–171, doi:10.1007/BF00307560.

Kern, H. (1982), P- and S-wave velocities in crustal and mantle rocks under the simultaneous action of high confining pressure and high temperature and the effect of the rock microstructure, in *High-Pressure Research in Geosciences*, edited by W. Schreyer, pp. 15–45, E. Schweizerbart'sche, Stuttgart, Germany.

Kern, H., and J. M. Tubia (1993), Pressure and temperature dependence of P- and S-wave velocities, seismic anisotropy and density of sheared rocks from Sierra Alpujata massif (Ronda peridotites, southern Spain), *Earth Planet. Sci. Lett.*, *119*, 191–205, doi:10.1016/0012-821X(93)90016-3.

Kern, H., S. Gao, and Q.-S. Liu (1996), Seismic properties and densities of middle and lower crustal rocks exposed along the North China Geoscience Transect, *Earth Planet. Sci. Lett.*, *139*, 439–455, doi:10.1016/0012-821X(95)00240-D.

Kern, H., S. Gao, Z. M. Jin, T. Popp, and S. Y. Jin (1999), Petrophysical studies on rocks from the Dabie ultrahigh-pressure (UHP) metamorphic belt, central China: Implications for the composition and delamination of the lower crust, *Tectonophysics*, *301*, 191–215, doi:10.1016/S0040-1951(98)00268-6.

Kern, H., Z. M. Jin, S. Gao, T. Popp, and Z. Q. Xu (2002), Physical properties of ultrahigh-pressure metamorphic rocks from the Sulu terrain, eastern central China: Implications for the seismic structure at the Donghai (CCSD) drilling site, *Tectonophysics*, *354*, 315–330, doi:10.1016/S0040-1951(02)00339-6.

Li, Y. Y., J. Downton, and B. Goodway (2003), Recent applications of AVO to carbonate reservoirs in the western Canadian sedimentary basin, *Leading Edge*, *22*, 670–674, doi:10.1190/1.1599694.

Lubarda, V. A. (1998), A note on the effective Lamé constants of polycrystalline aggregates of cubic crystals, *J. Appl. Mech.*, *65*, 769–770, doi:10.1115/1.2789122.

Mavko, G., T. Mukerji, and J. Dvorkin (2009), *The Rock Physics Handbook: Tools for Seismic Analysis in Porous Media*, 511 pp., doi:10.1017/CBO9780511626753, Cambridge Univ. Press, Cambridge, U. K.

Nadeau, J. C. (1999), A note on the effective Lamé constants of polycrystalline aggregates of cubic crystals, *J. Appl. Mech.*, *66*, 577.

Shapiro, S. A. (2003), Elastic piezosensitivity of porous and fractured rocks, *Geophysics*, *68*, 482–486, doi:10.1190/1.1567216.

Shen, A. H., W. A. Bassett, and I.-M. Chou (1993), The α-β quartz transition at high temperatures and pressures in a diamond-anvil cell by laser interferometry, *Am. Mineral.*, *78*, 694–698.

Spetzler, H. A., and D. L. Anderson (1968), The effect of temperature and partial melting on velocity and attenuation in a simple binary mixture, *J. Geophys. Res.*, *73*, 6051–6060, doi:10.1029/JB073i018p06051.

Stierman, D. J., J. H. Healy, and R. L. Kovach (1979), Pressure-induced velocity gradient: An alternative to a Pg refractor in the Gabilan range, central California, *Bull. Seismol. Soc. Am.*, *69*, 397–415.

Wang, Q., and S. C. Ji (2009), Poisson's ratios of crystalline rocks as a function of hydrostatic confining pressure, *J. Geophys. Res.*, *114*, B09202, doi:10.1029/2008JB006167.

Wang, Q., S. C. Ji, M. H. Salisbury, B. Xia, M. B. Pan, and Z. Q. Xu (2005a), Shear wave properties and Poisson's ratios of ultrahigh-pressure metamorphic rocks from the Dabie-Sulu orogenic belt: Implications for the crustal composition, *J. Geophys. Res.*, *110*, B08208, doi:10.1029/2004JB003435.

Wang, Q., S. C. Ji, M. H. Salisbury, M. B. Pan, B. Xia, and Z. Q. Xu (2005b), Pressure dependence and anisotropy of P wave velocities in ultrahigh-pressure metamorphic rocks from the Dabie-Sulu orogenic belt (China): Implications for seismic properties of subducted slabs and origin of mantle reflections, *Tectonophysics*, *398*, 67–99, doi:10.1016/j.tecto.2004.12.001.

Watanabe, T., H. Kasami, and S. Ohshima (2007), Compressional and shear wave velocities of serpentinized peridotites up to 200 MPa, *Earth Planets Space*, *59*, 233–244.

Zimmerman, R. W., W. H. Somerton, and M. S. King (1986), Compressibility of porous rocks, *J. Geophys. Res.*, *91*, 12,765–12,277, doi:10.1029/JB091iB12p12765.

S. Ji, D. Marcotte, and S. Sun, Département des Génies Civil, Géologique et des Mines, École Polytechnique de Montréal, Montréal, QC H3C 3A7, Canada. (sji@polymtl.ca)

Q. Wang, Key Laboratory of Marginal Sea Geology, Guangzhou Institute of Geochemistry, Chinese Academy of Sciences, Wushan, Guangzhou 510640, China. (wangqian@gig.ac.cn)